Shear waves with orthogonal polarisations for thickness measurement and crack detection using EMATs

Jaime Parra-Raad, Pouyan Khalili, Frederic Cegla[*]

NDE Group, Mechanical Engineering Department, Imperial College London, Exhibition Road, South Kensington SW7 2AZ, United Kingdom

ABSTRACT

The use of polarised shear waves to detect the presence of crack-like defects seems to have received little or no attention in the past. The authors believe that the main reason for this appears to be the lack of a device with the capability to excite shear waves of different polarisations. In this paper, the authors, first, present the design of an EMAT that permits the excitation of two orthogonally polarised shear waves in metallic materials by means of two coils that are orthogonal with respect to each other. This is then followed by a 3D finite element analysis of the wavefield generated by the EMAT and its interactions with crack-like defects of different sizes, positions and orientations. Then a methodology of how this EMAT can be used to simultaneously measure material thickness and detect crack-like defects in pulse-echo mode is introduced. Good agreement between the finite element simulation and experimental results was observed which makes the presented technique a potential new method for simultaneous thickness measurements and crack detection.

1. Introduction

Pulse-echo mode thickness measurements are one of the most commonly employed ultrasound non-destructive evaluation (NDE) techniques. The procedure consists in exciting 0° waves using an ultrasound transducer (UT). These waves propagate into the material that is to be inspected at an angle that is normal to the surface and reflect from the back-wall of the inspected component before returning to the transducer. The series of wave reflections and their time of flight (ToF) can be used to determine the thickness of the material at the specific spot where the UT is located [1,2]. Example applications where UTs are frequently used to inspect metallic materials are: manual thickness measurements [3–5], corrosion mapping [6,7] inline inspection (ILI) with e.g. pipeline inspection gauges (PIGs) [8,9] and permanently installed devices for thickness gauging [10–13].

The effectiveness of the thickness measurements depends on the quality of the returning signals. Severe surface roughness and non-uniformity can result in low signal to noise ratio (SNR) [14] and poor thickness measurements [15]. At the same time, ToF calculations of 0° wave reflections are relatively insensitive to small defects and crack-like defects because they reflect very little energy back and do not influence the arrival time of back-wall reflections [16]. These effects on the signal are, in some cases, comparable to the changes induced by surface roughness and therefore 0° waves are usually unsuitable for crack detection.

A different setup is used to perform crack detection with ultrasound [17]. An angled beam is sent into the inspected component; which is usually achieved by installing a piezo-electric UT onto an angled wedge [18]. The inspection consists in generating an ultrasound pulse that travels through the wedge and refracts at the wedge-specimen interface, resulting in an obliquely travelling wave in the material that is being inspected. The presence of a defect in the travel path of the wave can result in partial or complete reflection (depending on the geometry of the defect) of the ultrasound wave which reflects back to the transducer; therefore a defect is detected when a reflected signal is received [18,19]. Applications of these type of UT probe are: crack detection [19], and NDE inspection of train wheels [20].

The above shows that two different setups are required to perform thickness measurements and crack detection. This can be practically inconvenient to implement. Therefore, to overcome these impracticalities, in this work we investigated if both measurements can be combined by performing two simultaneous pulse-echo tests. The concept is to use a pair of orthogonal and linearly polarised shear waves emitted by the same transducer. This enables thickness gauging and crack-like defect detection with the same setup.

The UT probe that is presented in this paper consists of an electro-

---

magnetic acoustic transducer (EMAT) that contains two orthogonal co-located butterfly coils. The EMAT can excite a pair of perpendicular and linearly polarised shear waves propagating into the inspected material at 90° relative with its surface. The generated waves travel through the metallic material and bounce back from the back-wall to the transducer. The received back-wall reflections are analysed to quantify the thickness of the material and to determine the presence of a crack-like defect.

Thickness gauging is performed, using an orthogonal co-located coil (OCLC) EMAT, by calculating the ToF of the received back-wall reflections. While, the presence of crack-like defects is detected by comparing the amplitudes of the two orthogonal and linearly polarised shear wave reflections. This is possible because the amplitude of the reflected shear waves is strongly dependent on the relative orientation of a crack-like defect with respect to the polarisation direction of the incident shear wave.

There has been prior work aimed at understanding how linearly polarised shear waves interact with crack-like defects. For instance, S. K. Datta et al. [21] investigated how shear horizontal waves are diffracted when interacting with surface-breaking defects at different angles. Their experimental results indicated that SH waves propagating at 0° can be used to detect surface-breaking defects. A. H. Harker [22] analysed in-plane shear waves interacting with surface-breaking cracks at different incident angles. He concluded that in-plane incident shear waves split their energy into other waves after interacting with the defect. Howard [16] described qualitatively how the back-wall reflections of bulk waves are affected by the width of surface-breaking defects with respect to the UT aperture. In industry, for example, it is a well-established procedure to measure the arrival time of several oblique angle shear vertical wave reflections to size a crack-like defect [17]. However, there is no methodology that utilises relative changes in amplitude between orthogonal polarised shear waves to detect the presence of a crack-like defect. The authors believe that the lack of this methodology is a result of the absence of a device capable to record the amplitude of two orthogonal shear waves simultaneously, and also because there are no studies that relate the amplitude of shear wave reflections to the size of crack-like defects. Therefore, this is what we set out to investigate in this paper.

To understand how both 0° shear waves interact with back-wall cracks and how crack-like defects affect the reflected waves; 3D Finite Element (FE) simulations of the waves interacting with different crack-like defects were performed. An experimental setup that mimics the 3D-FE model was then built to validate the FE simulation results. The simulation and experimental results were compared and their agreement was verified.

This paper is organised as follows: in section 2, the OCLC EMAT layout is described. In section 3 we present the FE model used to study the interaction of the EMAT wavefield with notches of different sizes and orientations. In section 4, we explain the behaviour of the reflected waves when the EMAT wavefield interacts with crack-like defects and then we illustrate the concept of crack-like defect detection with FE simulation results. In section 5, the experimental design and setup is presented. In section 6 we compare the FE simulation results with their equivalent experimental measurement results. Section 7 discusses the presented work and its conclusion.

2. The orthogonal co-located coils (OCLC) EMAT

The authors of this paper are proposing to use an EMAT that contains a pair of orthogonal co-located coils (schematic concept of the magnetic flux orientation, the orthogonal coil design and the directions of the generated shear forces are shown in Fig. 1a and b). The design of the proposed EMAT is based on the results presented by Ref. [12]. The EMAT that they designed maximised the bias magnetic field, so that, in combination with one butterfly coil (20 turns, 0.25*mm* track width and 0.25*mm* gap between tracks), it generates a linearly polarised 0° shear
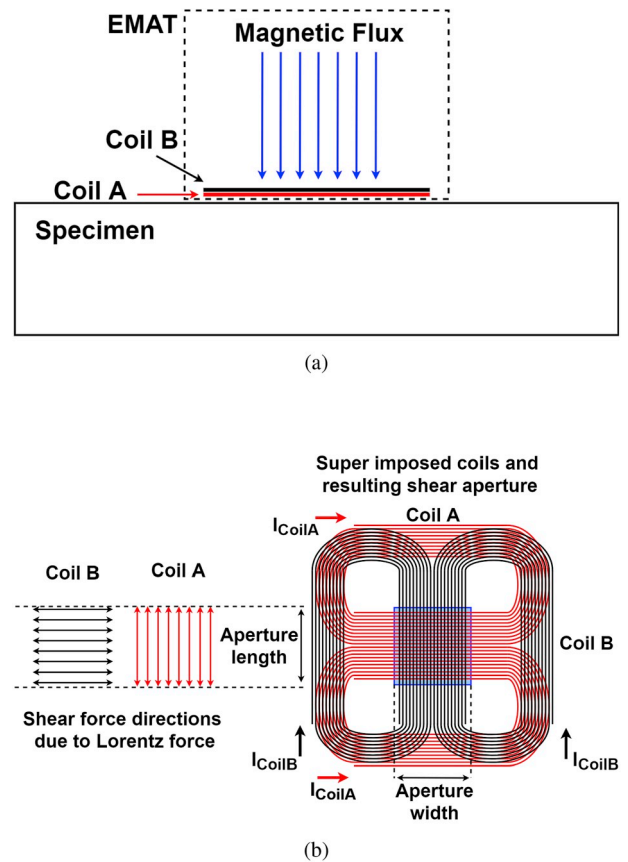

(a)

(b)

Fig. 1. Schematic of the orthogonal co-located EMAT coils. a) Schematic side view of the OCLC EMAT. b) Top view layout showing the two coils that are identical but rotated by 90° and placed on top of each other, as well as the active aperture area and the shearing direction resulting from the two coils. I*CoilA* and I*CoilB* indicate the current direction in the coils.

wave by means of the Lorentz force mechanism [23]. The OCLC EMAT its composed of the same magnetic circuit and coil introduced by Ref. [12] plus a second identical butterfly coil that is placed on top and rotated at 90° relative to the first EMAT coil. Both coils are placed at the bottom of the EMAT. Therefore, the description of the magnetic field and the ultrasound wave generation of the OCLC EMAT is the same to the one described by Isla et al. but with the difference that an additional ultrasound shear wave with perpendicular polarisation direction is generated by the second coil. Therefore, the active aperture of the OCLC EMAT is a square area at its centre (marked in blue in Fig. 1b) [16] where the vertical and horizontal tracks of the coils cross. It is in this area where the magnetic flux is applied and hence where the Lorentz force will exert a surface traction on the specimen.

3. Finite element simulation of interaction of SH waves with notches/cracks in isotropic materials

In order to assess the interaction of the two orthogonal and linearly polarised shear waves with crack-like defects of various depths, widths and orientations, FE analysis was employed. FE is a versatile and powerful tool that allows the investigation of a large number of defect shapes/sizes which would be very costly to fully examine experimentally.

The predictions were performed in a pulse-echo setup at 2 MHz centre frequency, which in an aluminium ($\rho = 2700kg/m^3$, $E = 70.76GPa$, $\nu = 0.3375$) structure corresponds to a wavelength of around 1.6*mm*. The full 3D FE simulations were carried out with the Pogo Software package [24]. Which is a FE simulation package dedicated to

solving explicit time domain wave propagation problems [25]. In order to ensure the accuracy and stability of the simulations, cubic elements with side lengths of 0.05*mm* and a time step of 6.34*ns* were used. To ensure the simulations use the least possible computation resources, a small section of a block was modelled. The geometry investigated through out the simulations is shown in Fig. 2. Here, a typical model had around 648 million degrees of freedom and took approximately one hour and half to run on a data Muncher with 8 Nvidia Quadro RTX 8000 GPU cards.

Fig. 2 displays the general FE setup used throughout this study. In order to mimic the OCLC EMAT active area, an excitation area of 12*mm* x 12*mm* [16] was placed on the top surface of a 30*mm* thick aluminium block where polarised shear waves were generated via tangential surface tractions; the excitation signal consisted of a 5-cycle Hanning-windowed toneburst at 2*MHz* centre frequency with maximum amplitude of 1, (The authors are assuming that the wave propagation of the shear waves is a linear problem and are only interested in relative amplitude changes of the waves. Therefore, the absolute values of the surface tractions in the simulations are not relevant for the results of this study). The preference of the authors to use a 5-cycle Hanning-windowed toneburst rather than a single pulse as an excitation signal is due to its well-defined frequency bandwidth compare to single pulse signals. The surface defect was placed on the opposite surface of the aluminium block. By simply changing the geometry of the defect, the effect of various parameters such as defect depth, width and orientation on the reflection of the shear waves can be studied.

To simulate a pulse-echo measurement, the reflection was recorded via the same nodes used for the excitation (red area in Fig. 2) where the OCLC EMAT reception was simulated by summing and then normalising the surface displacement components oriented along the corresponding coil direction.

In order to understand the behaviour of the polarised shear waves when interacting with surface crack-like defects, an one-element-wide notch defect was placed at the middle of the block, as is shown in Fig. 2. The defect was created by disconnecting the set of nodes at the location of the discontinuity. With this configuration, the displacement coming from the left-hand side of the defect is not transferred to the right-hand side and vice versa, simulating the effect of a surface-breaking defect. Then, simulations of the wave propagation were carried out with various defect depths (0.05, 0.3, 0.5, 1, 2, 3, 4, 5, 6, 7, 8, 9 and 10*mm*) as well as for different normalised (to transducer size) defect lengths of 5%, 10%, 20%, 40%, 60%, 80% and 100% and at different orientations (0°, 10°, 20°, 30°, 40°, 45°, 50°, 60°, 70°, 80° and 90°).
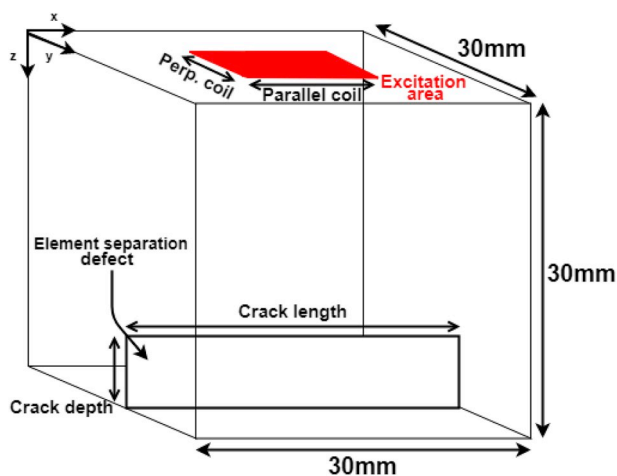

Fig. 2. Schematic of the FE setup. The red area represent the equivalent OCLC EMAT excitation/reception area (aperture). (For interpretation of the references to colour in this figure legend, the reader is referred to the Web version of this article.)

4. Measurement concept

The procedure of measuring the thickness of a metallic material consists in generating an ultrasound wave at the material surface, and then recording the reflections of the emitted wave from the back-wall of the material. By determining the ToF between consecutive back-wall reflections and multiplying this with the wave speed, the thickness of the material is estimated.

Moreover, to detect the presence of crack-like defects, the relative amplitude of the reflection of two orthogonal and linearly polarised shear waves that are co-located is proposed. This is possible because the reflected amplitude of a transmitted linearly polarised shear wave through an area of material containing a crack-like defect is strongly dependent on the relative orientation of the defect and the incident shear wave polarisation. Fig. 3 illustrates how the shear waves are affected by the presence of a crack-like defect. The FE simulation results were obtained for a notch of 0.05*mm* width, 5*mm* depth and 30 mm length. Fig. 3a shows how an incident shear wave that has a polarisation direction parallel to the defect face is almost unaffected by the presence of the notch, while Fig. 3b illustrates how an incident shear wave with polarisation perpendicular to the notch scatters at the defect's tip and mode converts into compression and Rayleigh waves. Fig. 3c shows the amplitude of the signals recorded when the incident shear wave is parallel or perpendicular to the notch orientation. The time-traces show the excitation signal used for the pulse-echo tests, the received L + S wave which is the resultant wave of the mode conversion of the longitudinal wave that is excited at the edges of the OCLC EMAT's aperture and then mode converted to shear waves at the back-wall surface of the specimen [12] and the 1st back-wall reflection recorded at the aperture area. The amplitude difference between both 1st back-wall reflections is due to the relative orientation of the shear waves with respect to the notch.

The amplitude of a reflected shear wave when interacting with a crack-like defect also depends on the relative length of the defect with respect of the transducer aperture. If the crack-like defect is shorter/smaller than the transducer aperture, part of the incident wave will not interact with the defect, leaving the reflected wave from that area unaffected by the presence of the defect. Fig. 4 shows the back-wall reflection amplitude drop of the shear wave perpendicular to the defect as a function of the crack depth and aperture. The results show that the amplitude drop increases for deeper and/or longer defects.

The amplitude drop is also dependent on the width of the defect/notch as additional scattering occurs due to the reflection from the top side of the defect; hence higher amplitude is observed as the width of the defect is increased. Fig. 5 displays the effect of the crack-like defect (notch) width on the amplitude drop of back-wall reflections. The FE results show the percentage of amplitude drop of the perpendicular and parallel (relative to the defect face) shear waves as a function of the defect/notch width ranging from 0 to 1 *mm*.

The OCLC EMAT, in pulse-echo mode, is proposed to be used to measure the thickness of a metallic material and detect the presence of a crack-like defect in the same material by exciting two orthogonal and linearly polarised shear waves simultaneously. The two generated shear waves will interact with the material back-wall surface and reflect towards the OCLC EMAT. The thickness of the material is proposed to be measured by calculating the ToF using one of the signals recorded with the coils. To detect the presence of a crack like defect, the amplitudes of the two reflected waves could be recorded and compared to each other. If there is an amplitude drop in one of the waves relative to the other, then it has been detected that one of the incident waves has scattered more energy away due to the presence of an anomaly in the material. Which is most likely the result of the presence of a notch or crack-like defect.
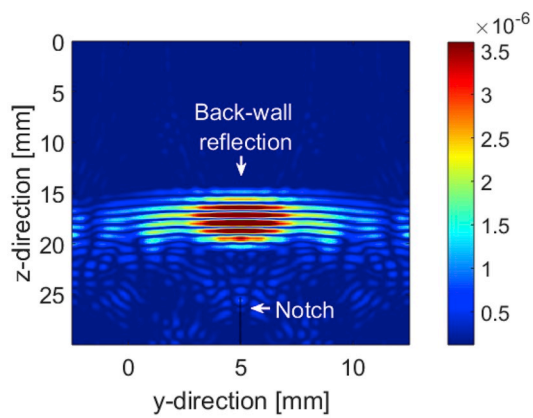
(a)
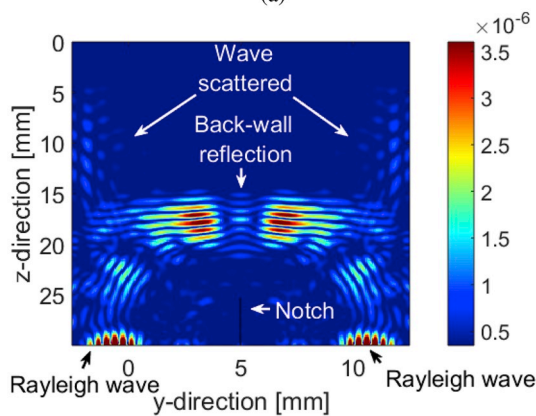
(b)
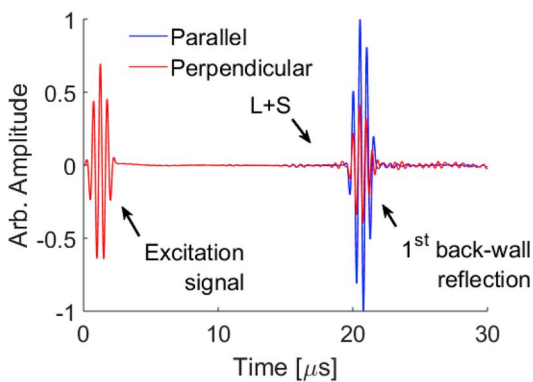
(c)

Fig. 3. FE results of two orthogonal and linearly polarised shear waves (2 MHz, 5-cycle Hanning-windowed) interacting with a notch defect of $0.05mm$ width and $5mm$ depth across the back surface of the material. a) Displacement magnitude of the shear wave with polarisation aligned parallel. b) Displacement magnitude of the shear wave with polarisation aligned perpendicular. c) Normalised time-trace of the incident and reflected shear waves when the back-wall has a notch in it.

5. Experiment design and setup

To verify the FE predictions, an OCLC EMAT with $12mm$ active aperture was built and placed on a $30mm$ thick, $250mm$ long and $100mm$ wide aluminium block. Three notches with different depths (0.3, 1 and $5mm$ as shown in Fig. 6a) were machined into the back-wall of the block. The notches were $0.3mm$ wide and spanned the whole width of the specimen. Then, four different experiments were carried out by performing several pulse-echo tests on the aluminium block. The first
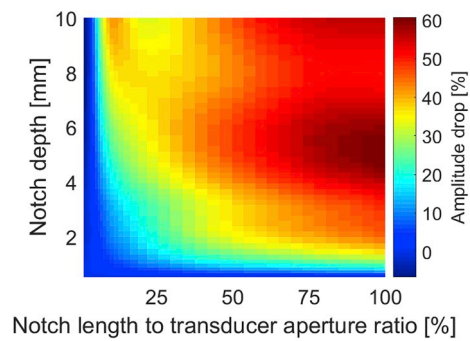

Fig. 4. FE simulation predictions of the amplitude drop of the perpendicularly (with respect to defect face) and linearly polarised shear wave relative to the parallel polarised shear wave as a function of crack depth and crack length. The results were obtained for a $30mm$ thick aluminium block at a centre frequency of $2MHz$.
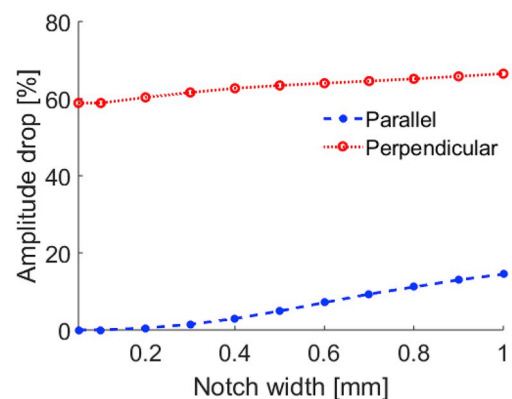

Fig. 5. FE simulation results of the notch width effect in the percentage amplitude drop of linearly polarised shear wave back-wall reflections. The notches simulated were $30mm$ long and $5mm$ depth.

experiment, which consisted in a pulse-echo test executed in a defect free region (OCLC EMAT placed at $100mm$ as shown in Fig. 6a), was carried out to get the baseline amplitude of the reflected shear waves and the wave propagation velocity of the excited shear waves. The second experiment consisted of a pulse-echo test over the three different notches (where one of the linearly polarised shear waves was aligned parallel with the notch orientation), the purpose of this experiment was to measure the effect of defect depth in the amplitude of the reflected shear waves. The results obtained in the first and second experiment were analysed to extract the back-wall reflection amplitude drop due to the presence of the notches and the estimated thickness of the material when a defect is present. The third experiment was performed to investigate the effect of the transducer offset relative to the defect position. The experiment was conducted by varying the relative offset between the $5mm$-depth notch and the centre of the OCLC EMAT. The relative offset was varied from -10 to $10mm$ with a $1mm$ step. The last experiment was performed to measure the amplitude drop when the relative orientation of the OCLC EMAT with respect to the defect is varied. The experiment was executed by rotating the OCLC EMAT in $10°$ steps from $90°$ position to the $0°$ position. For the four experiments both coils were used in pulse-echo mode; and the coils were exited simultaneously. Fig. 6a depicts the geometrical setup of the first three experiments and Fig. 6b shows the geometrical setup of the last measurement.

A schematic of the experimental setup used to perform the experiments is shown in Fig. 7a. The measurement setup consists of a computer, a data acquisition system (DAQ) containing two synchronised Handyscope-5 (HS5) with arbitrary function generator (AWG) and oscilloscopes, an Amplification System (AS) developed in-house and the
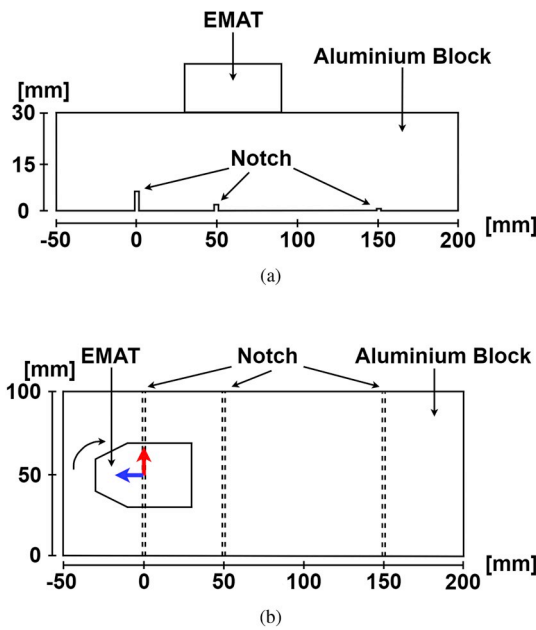
Fig. 6. Schematic of the measurement setup and geometrical orientation of the OCLC EMAT. a) Front view. b) Top view. Arrows indicates the coils orientation when the OCLC EMAT has a angle rotation of 0° with respect of the notch. Blue arrow represents coil A orientation and red arrow indicates coil B orientation. (For interpretation of the references to colour in this figure legend, the reader is referred to the Web version of this article.)
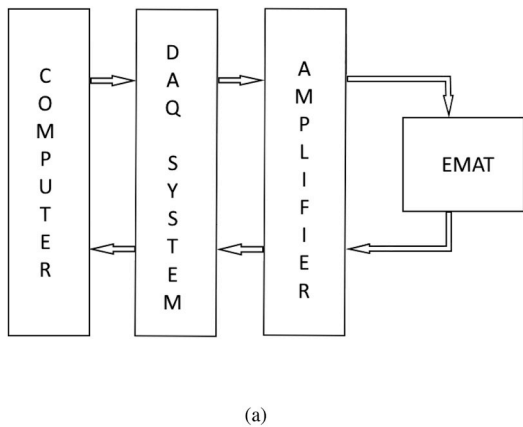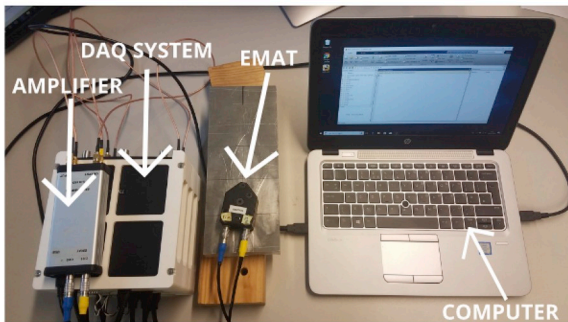
Fig. 7. Measurement setup. a) Schematic. b) Picture of the full acquisition system including Laptop, HS5, Amplifier, specimen and OCLC EMAT.

OCLC EMAT. A picture of the full system is shown in Fig. 7b.

The computer, which controlled the experiment, executed a Matlab [26] routine that used two synchronised HS5 devices to send and receive signals to/from each coil. Inbetween the HS5s and the OCLC EMAT the AS was connected. The purpose built amplifier was used to enhance the excitation and receive signals of the transducer. The AS contains a buffer amplifier on the transmitting side, an isolation switch to interchange between transmitter and a 60 *dB* receiver amplifier.

Ultrasound data could be acquired rapidly and simultaneously from both OCLC EMAT coils by employing the use of coded sequences to excite each coil [27]. The signal encoded was a 5-cycle Hanning-windowed toneburst at 2*MHz* centre frequency with an amplitude of 24V_{pp} from the AWG. Then, the signal was amplified by the AS and transmitted to the OCLC EMAT, which induced the tangential traction at the surface of the aluminium block. Once the ultrasound signal has been excited and travelled through the material, its reflections from the back-wall of the material were measured by the OCLC EMAT and sent to the AS, which amplified the received signal to be recorded by the HS5 devices.

6. FE and experimental results

The results of two pulse-echo test on the aluminium block, using the OCLC EMAT, are shown in Fig. 8. The time-traces shown in Fig. 8a are the results of the inspection when the OCLC EMAT is placed on top of the undamaged area of the aluminium block and Fig. 8b shows the results of the inspection when the OCLC EMAT is placed on top of the 5*mm*-depth notch.

The ToFs shown in Table 1 were calculated by measuring the time difference among maximum absolute values of the 1st and 2nd back-wall reflection of the same time-trace. The ToF calculated, when the back-wall is undamaged, were used to estimate the reference values of the shear wave propagation velocities in the aluminium block at the
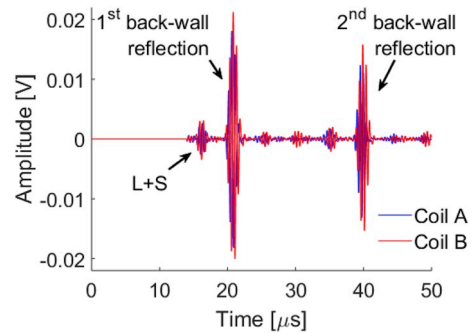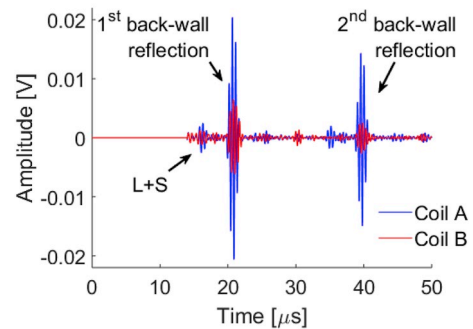
Fig. 8. Back-wall reflection recorded with the OCLC EMAT coils. a) Back-wall reflection from an undamaged back surface. b) Back-wall reflection when a 5*mm* depth, 0.3*mm* width and 100*mm* long notch is present.

Table 1
Estimated velocity and thickness using the OCLC EMAT.

Thickness measurement			
		Undamaged	Notch present
Coil A	ToF	18.88μs	19.04μs
	SW velocity	3178m/s	3178m/s
	Thickness	30mm	30.03mm
Coil B	ToF	18.9μs	19.06μs
	SW velocity	3151m/s	3151m/s
	Thickness	30mm	30.03mm

Fig. 10. Maximum amplitude drop of the back-wall reflection vs offset distance between notch and OCLC EMAT. The experimental results are the result of the shear waves interacting with the 5mm-depth notch, while for the FE, the results are from the interaction with a 0.05mm-width and 5mm-depth notch. The amplitude drop percentage was calculated by comparing the results when the defect is present and absent.

direction of each coil. The velocities were calculated by dividing the distance that the shear waves travelled in the aluminium block by the ToF.

Once the shear wave propagation velocities in the aluminium block were estimated, the calculated ToFs when the notch is present were used to measure the thickness of the aluminium block. The thickness was measured by multiplying the ToFs with the shear wave propagation velocities in aluminium and then divide the result by the times that the wave travelled through the material from the 1st to 2nd back-wall reflection. The estimated velocities and thicknesses using the calculated ToFs when the back-wall of the aluminium block is undamaged and when the notch is present are shown in Table 1.

The results of the second, third and last experiments with their equivalent FE results are shown in Figs. 9–11 respectively. The FE results in Figs. 9–11 were obtained for 0mm-width notches, while the experimental results were obtained for 0.3mm-width notches. The rest of the geometrical dimensions of the notches were the same for both cases.

Fig. 9 shows the maximum amplitude drop of the shear waves as a result of their interaction with notches of different depth. Fig. 10 shows the relative amplitude drop from each coil as a function of OCLC EMAT offset relative to the notch (0mm value offset signifies that the OCLC EMAT is directly over the defect). Fig. 11 shows the results acquired in the fourth experiment. The normalised maximum amplitude recorded on both coils is plotted for each angular position in which it was taken. The amplitude drop percentage for Figs. 9 and 10 were calculated by comparing the results to those obtained from the undamaged section of the specimen.
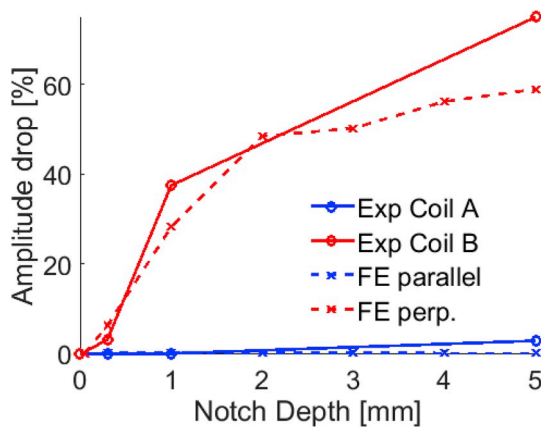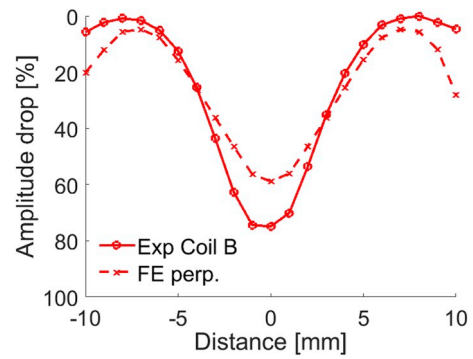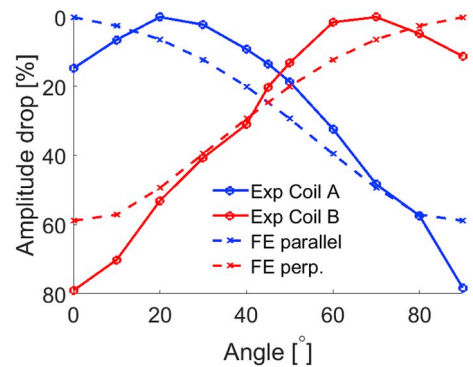

Fig. 11. Maximum amplitude of the back-wall reflection vs relative angle of the 5mm-depth notch with the OCLC EMAT. The experimental results are the result of the shear waves interacting with the notch, while for the FE, the results are from the interaction with a 0.05mm-width notch. The amplitude drop percentage was calculated by measuring how much each amplitude data point has decreased compare with the maximum value in the experiment.

7. Discussion

The capabilities of the OCLC EMAT towards the detection of crack-like defects were established. In all cases, it was found that experimental results show good agreement to the corresponding FE prediction. It should be noted, however, that the majority of the FE results were obtained for 0.05mm-width notches hence the lower predicted amplitude drops compared to the experimental measurements. Other factors such as surface roughness associated with the notches faces and a no perfectly flat bottom surface of the notches were thought to further enhance the amplitude drop recorded in experiments.

The amplitude drop percentage recorded with the OCLC EMAT depends on the relative position and orientation of the coils with respect to the crack-like defect; and therefore the highest chance to detect the presence of the defect occurs when one is positioned directly above the defect and oriented perpendicular to the defect. However, if the relative orientation of both coils with respect of the defect is similar (close to 45°), then the amplitude drop of each coil will be similar, complicating the detection of the defect. In such cases, the presence of the defect can be verified by rotating the transducer in the same position which enables higher contrast between the amplitude drops recorded by each OCLC EMAT coil.

The capability to perform thickness measurements using the OCLC EMAT was verified by estimating the thickness of an aluminium block

Fig. 9. Maximum amplitude drop of the back-wall reflection vs the depth of a notch. The experimental results are the result of the shear waves interacting with different 0.3mm-width notches, while for the FE, the results are from the interaction with different 0.05mm-width notches. The amplitude drop percentage was calculated by comparing the results when the defect is present and absent.

when the back-wall surface was undamaged and when a crack-like defect was present. The experimental results of thickness measurement are presented in Table 1 and Fig. 8. The results, for each coil, show similar estimation values for both cases; showing that the thickness measurement can be performed irrespective to the presence of a crack-like defect. However, slight difference between the ToFs recorded by each of the coils was found to be due to the material anisotropy of the tested aluminium block, resulting in wave velocity variation of around 1%. This discrepancy can be compensated for by comparing the ToFs recorded by each coil when obtained on an undamaged section of the specimen.

Moreover, there is a $0.02\mu s$ difference among ToFs measured with the same coil (when the notch is present and when back-wall surface is undamaged). This difference corresponds to a position change of the maximum peak of the back-wall reflections of 1 sample, at the sampling frequency of $50MHz$, and is therefore not believed to be significant as slight changes in amplitude and noise can push the peak into the next digital sample point.

8. Conclusion

This paper has demonstrated that EMATs containing orthogonal co-located coils can be used to excite two perpendicular and linearly polarised shear waves. The two perpendicularly oriented shear waves interact very differently with crack-like defects and the resulting amplitude difference of the received signals can be used as a reliable indicator for the presence of a defect in metallic materials. The results obtained with the OCLC EMAT show that crack-like defects with depth $0.3mm$ (0.2λ) or higher can be detected by placing one of the shear waves parallel to the defect face and comparing the maximum amplitude difference between the signals that are measured with both coils. However, the received signal amplitude drop plateaus at a crack depth of roughly 2λ, meaning the amplitude drop value cannot be used to estimate the size of defects of $3mm$-depth or larger. Additionally, the amplitude drop of the recorded back-wall reflections depends of the relative orientation and position of the OCLC EMAT with respect to the crack-like defect. The chance to detect the presence of a crack-like defect decreases when the OCLC EMAT is not on top nor aligned with the direction of the defect.

To investigate how the amplitude of the received signals can be used to determine the presence of a defect, FE simulations of the two orthogonal and linearly polarised shear waves interacting with different crack-like defects were performed and validated with experimental results. The FE and the experimental results show good agreement. The discrepancies resulted because the FE simulations were performed for $0.05mm$-width notches while the experiments where implemented on notches with a finite width.

The NDE technique introduced in this paper is a new concept that can be used for thickness measurements and crack-like defect detection. The advantage of this technique with respect of conventional NDE techniques is that one single setup allows to perform both measurements simultaneously.

References

[1] ASTM E797/E797M-10. Standard practice for measuring thickness by manual ultrasonic pulse-echo contact method, standard. West Conshohocken, PA, USA: ASTM International; 2015.

[2] BS EN 141227. Non-destructive testing-Ultrasonic thickness measurement, Standard. London, UK: British Standard Institution; 2011. 2013.

[3] Kobayashi M, Jen C-K, Bussiere J, Wu K-T. High-temperature integrated and flexible ultrasonic transducers for nondestructive testing. NDT E Int 2009;42: 157–61.

[4] Dixon S, Edwards C, Palmer S. High accuracy non-contact ultrasonic thickness gauging of aluminium sheet using electromagnetic acoustic transducers. Ultrasonics 2001;39:445–53.

[5] Robinson A, Drinkwater B, Allin J. Dry-coupled low-frequency ultrasonic wheel probes: application to adhesive bond inspection. NDT E Int 2003;36:27–36.

[6] Benstock D, Cegla F, Stone M. The influence of surface roughness on ultrasonic thickness measurements. J Acoust Soc Am 2014;136:3028–39.

[7] Brizuela J, Camacho J, Cosarinsky G, Iriarte J, Cruza J. Improving elevation resolution in phased-array inspections for ndt. NDT E Int 2019;101:1–16.

[8] Vanaei H, Eslami A, Egbewande A. A review on pipeline corrosion, in-line inspection (ili), and corrosion growth rate models. Int J Press Vessel Pip 2017;149: 43–54.

[9] Xie M, Tian Z. A review on pipeline integrity management utilizing in-line inspection data. Eng Fail Anal 2018;92:222–39.

[10] Honarvar F, Salehi F, Safavi V, Mokhtari A, Sinclair AN. Ultrasonic monitoring of erosion/corrosion thinning rates in industrial piping systems. Ultrasonics 2013;53: 1251–8.

[11] Cawley P, Cegla F, Stone M. Corrosion monitoring strategies—choice between area and point measurements. J Nondestruct Eval 2013;32:156–63.

[12] Isla J, Cegla F. Optimization of the bias magnetic field of shear wave emats. IEEE Trans Ultrason Ferroelectr Freq Control 2016;63:1148–60.

[13] F. Cegla, J. Allin, Ultrasonic monitoring of pipeline wall thickness with autonomous, wireless sensor networks, John Wiley & Sons, Ltd, pp. 571–578.

[14] Chen J, Shi Y, Shi S. Noise analysis of digital ultrasonic nondestructive evaluation system. Int J Press Vessel Pip 1999;76:619–30.

[15] Cegla F, Jarvis A. Modeling the effect of roughness on ultrasonic scattering in 2d and 3d. AIP Conf. Proc. 2014;1581:595–601.

[16] Howard RD. Quantitative evaluation of ultrasonic techniques for the detection and monitoring of corrosion in pipes. d. eng thesis,. Imperial College London; 2017.

[17] ASTM E2192-13. Standard guide for planar flaw height sizing by ultrasonics, standard. West Conshohocken, PA, USA: ASTM International; 2018.

[18] Ermolov IN. Progress in the theory of ultrasonic flaw detection. problems and prospects. Russ J Nondestruct Test 2004;40:655–78.

[19] Mak D. Ultrasonic methods for measuring crack location, crack height and crack angle. Ultrasonics 1985;23:223–6.

[20] Pohl R, Erhard A, Montag H-J, Thomas H-M, Wüstenberg H. Ndt techniques for railroad wheel and gauge corner inspection. NDT E Int 2004;37:89–94.

[21] Datta SK, Shah AH, Fortunko CM. Diffraction of medium and long wavelength horizontally polarized shear waves by edge cracks. J Appl Phys 1982;53:2895–903.

[22] Harker AH. Numerical modelling of the scattering of elastic waves in plates. J Nondestruct Eval 1984;4:89–106.

[23] Kawashima K, Wright OB. Resonant electromagnetic excitation and detection of ultrasonic waves in thin sheets. J Appl Phys 1992;72:4830–9.

[24] Huthwaite P. Pogo 2019. https://www.http://www.pogo.software.com.

[25] Huthwaite P. Accelerated finite element elastodynamic simulations using the GPU. J Comput Phys 2014;257:687–707. Part A.

[26] MathWorks Inc.. Matlab r2018b. 2018. https://www.mathworks.com/products/matlab.html.

[27] Isla J, Cegla F. Coded excitation for pulse-echo systems. IEEE Trans Ultrason Ferroelectr Freq Control 2017;64:736–48.